Effects of the Orion Launch Abort Vehicle Plumes on Aerodynamics and Controllability

Darby Vicker, Aerospace Engineer, NASA JSC, Professional Member AIAA
Robert Childs, Senior Research Scientist, STC
Stuart E. Rogers, Aerospace Engineer, NASA ARC, Associate Fellow AIAA
Matthew McMullen, Senior Research Scientist, STC, Senior Member AIAA
Joseph Garcia, Aerospace Engineer, NASA ARC, Senior Member AIAA
Jim Greathouse, Aerospace Engineer, NASA JSC

Characterization of the launch abort system of the Multi-purpose Crew Vehicle (MPCV) for control design and accurate simulation has provided a significant challenge to aerodynamicists and design engineers. The design space of the launch abort vehicle (LAV) includes operational altitudes from ground level to approximately 300,000 feet, Mach numbers from 0-9, and peak dynamic pressure near 1300psf during transonic flight. Further complicating the characterization of the aerodynamics and the resultant vehicle controlability is the interaction of the vehicle flowfield with the plumes of the two solid propellant motors that provide attitude control and the main propulsive impulse for the LAV. These interactions are a function of flight parameters such as Mach number, altitude, dynamic pressure, vehicle attitude, as well as parameters relating to the operation of the motors themselves – either as a function of time for the AM, or as a result of the flight control system requests for control torque from the ACM.

This paper discusses the computational aerodynamic modeling of the aerodynamic interaction caused by main abort motor and the attitude control motor of the MPCV LAV, showing the effects of these interactions on vehicle controllability.

Nomenclature

Eff_{Cm}	Pitching Moment Effectiveness
ACM	Attitude Control Motor
AM	Abort Motor
AMC_T	Abort Motor Thrust Coefficient
C_D	Drag Coefficient
C_m	Pitching Moment Coefficient
C_m-alpha	Pitching Moment Coefficient slope with respect to alpha
C_T	Thrust Coefficient
CFD	Computational Fluid Dynamics
CM	Crew Module
LAT	Launch Abort Tower
LAV	Launch Abort Vehicle
MPCV	Multi Purpose Crew Vehicle
SA	Spacecraft Adapter
SM	Service Module
WTT	Wind Tunnel Testing

I. Introduction

A. MPCV Components

The Orion Multi-purpose Crew Module (MPCV) is a system being designed to carry humans to exploration destinations beyond low-earth orbit and allow them to return safely. The MPCV system, pictured in Figure 1, consists of the Crew Module (CM), the Service module (SM), the Launch Abort Tower (LAT), and the spacecraft adapter (SA).

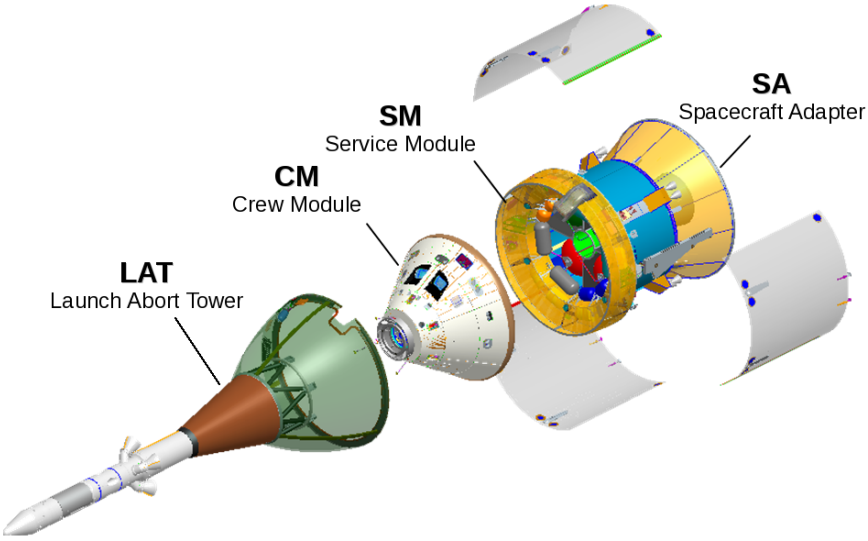

Figure 1. Major components of the MPCV

The CM provides the crew with habitable volume for all phases of flight including launch, spaceflight, and earth re-entry. As such, the CM is the central focus of the MPCV system with the other components designed largely to help the CM perform its mission. As a result, the CM contains a large number of the critical systems of the MPCV including the command and control functions, life support, etc. Systems placed on the other MPCV components are not needed for earth re-entry/landing and hosting off of the the CM allows the landed mass to be reduced, which simplifies the design of both the thermal protection and parachute systems.

The SM provides many functions for the MPCV. It provides all on-orbit attitude control and propulsion - including final ascent trajectory maneuvers and the deorbit impulse, electrical power generation via solar panels and electrical storage, heat rejection via radiators, consumable storage (e.g. oxygen, water, etc.), and ascent abort capability after the LAT is jettisoned. For nominal missions the SM is separated from the CM just before atmospheric re-entry and burns up in the atmosphere. During launch vehicle ascent, the SM is protected by panels that are jettisoned after first stage burnout. Jettisoning of these panels reduces the mass carried to orbit, and uncovers the SM radiators to allow rejection of heat produced by the CM systems.

The Spacecraft Adapter (SA) primarily serves to allow the MPCV system to be mounted atop the launch vehicle upper stage. The SA remains attached to the launch vehicle second stage after ascent.

The LAT protects the CM from ascent environments, but its main purpose is to provide the ability to pull the CM away from a failing launch vehicle or any danger on the launch pad and allow the CM to deploy parachutes and land safely. During an abort the LAT and CM remain coupled, and the CM detaches from the SM. This LAT+CM configuration is referred to as the Launch Abort Vehicle (LAV). The main propulsive force is provided by the Abort Motor (AM) mounted immediately forward of the CM in the LAT tower and provides up to 400,000 lbs of thrust through 4 nozzles canted 25 deg from the tower centerline and burns at high thrust for approximately 4 seconds with total burn time of approximately 7 seconds. The high thrust of the AM is designed to quickly accelerate the LAV away from the pad or launch vehicle danger and propel the CM to a safe distance. The design goal is to provide a minimum of 300 feet of separation from a launch vehicle that continues to accelerate three seconds from the abort initiation, and/or to provide sufficient altitude and downrange distance to allow safe parachute deployment and landing. Control of the

LAV is achieved by use of the Attitude Control Motor (ACM) mounted just aft of the nosecone and directs thrust through eight radially oriented nozzles that can independently vary the throat area. This allows the flight control system to command thrust magnitude from zero to approximately 7000lbs and orient the resultant thrust radially through 0-360 deg of azimuth. Since the ACM, like the AM, is a solid propellant motor it is always burning, to achieve resultant thrust less than maximum, opposing nozzles are opened to partially or fully cancel thrust produced by the primary nozzles. This ability to control thrust magnitude and direction allows the flight control to achieve the desired attitude of the LAV as it flies away from the a safe distance. After the initial fly-out and the LAV has slowed sufficiently, the ACM is used to re-orient the LAV from tower-forward flight to base-forward flight so that the CM heatshield faces into the freestream flow. This mimics a nominal entry attitude and allows the recovery system to be used for aborts without extensive modification after the LAT is jettisoned. Figure 2 gives an overall layout of the LAV showing the location of the ACM nozzles at the tip of the tower just below the nosecone, and the AM nozzles near the midpoint of the tower pointed aft at a 25 deg angle relative to the centerline.

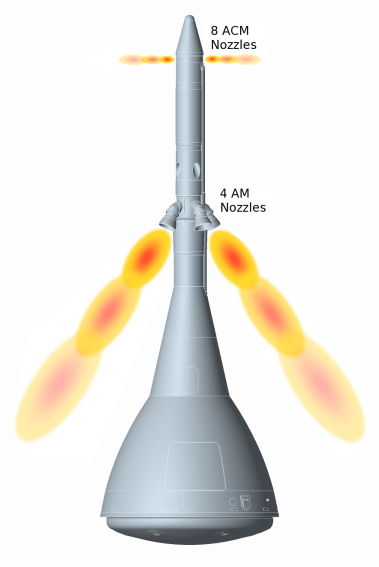

Figure 2. Location and orientation of the LAV AM and ACM nozzles

B. MPCV Ascent Abort Trajectory

For this paper we will focus on the LAV aborts, which take place from the launch pad throughout first stage flight of the launch vehicle. The LAT systems were designed with specifications that would allow aborts from the now canceled Ares 1 launch vehicle. The Ares 1 first stage burned for approximately 150 seconds, at which time it was separated, and the second stage was ignited to propel the MPCV to a transfer orbit with the SM performing the final orbital insertion burn. During the second stage flight, thrust can be terminated reliably and aerodynamic drag force has dropped to nearly zero due to the very high altitude. As a result the lower thrust of the service module main engine is capable of performing the needed abort propulsion. This allows the weight of the LAT to be jettisoned shortly after the second stage is ignited and verified to be operating properly.

The ascent trajectory of the solid propellant Ares I launch vehicle complicated the LAV design and analysis in many ways since the nominal ascent trajectory reached 900+ psf with the LAV accelerating to nearly 1300psf in some cases due to the AM thrust impulse. Figure 3 shows representative trajectory data from the LAV aborting off of a notional Ares 1 trajectory. The the circular symbols represent the starting point of the abort in Mach and dynamic pressure parameters when the AM and ACM are ignited and the LAV is separated from the SM to begin flying away from the launch vehicle. The black line indicates the LAV flight away from the launch vehicle while the AM is developing high thrust, then slowing as the drag exceeds thrust of the AM during its lower thrust and tail-off. The cyan line then continues the trajectory showing the period of time when the ACM is capable of approximately 7000 lbs thrust, while the red line shows

flight during the time the ACM is in its reduced thrust mode. The design of the ACM thrust profile was to provide high thrust when dynamic pressures and large disturbance torques are expected, and is reduced by approximately 65% thrust to allow longer burn time during the period of flight where lower dynamic pressures and thus disturbance torques are expected.

Through use of the LAT for aborts until the launch vehicle second stage, and use of the SM throughout second stage and orbital flight, the MPCV is able to provide abort capability at any point before or during the ascent flight, greatly enhancing crew safety.

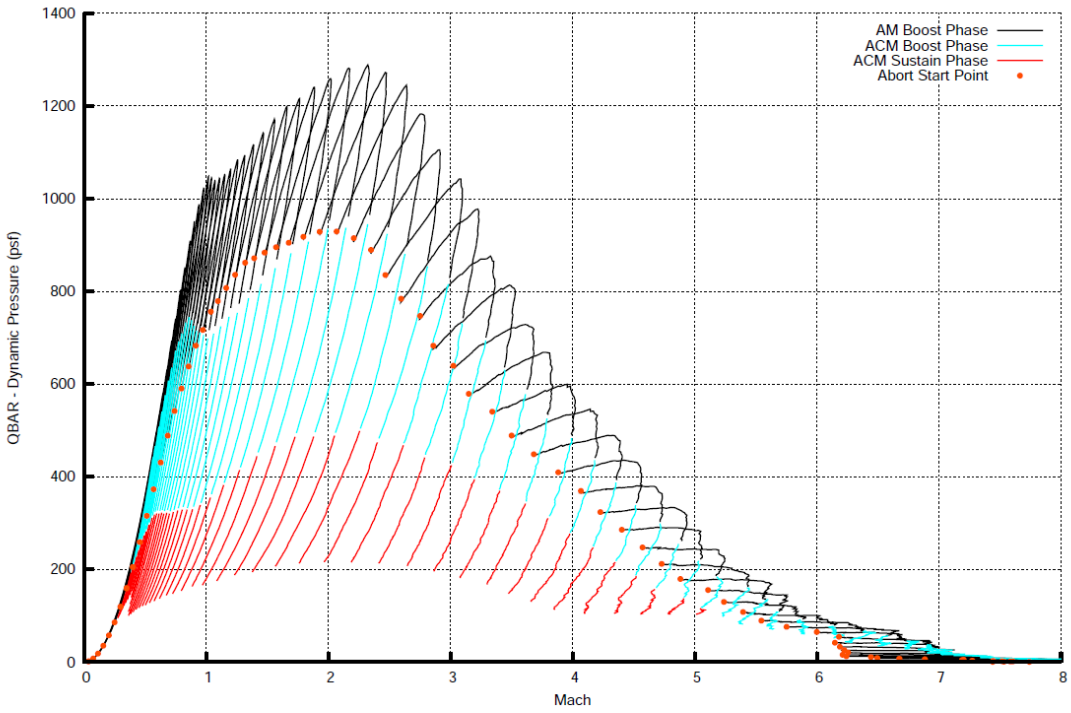

Figure 3. MPCV Abort Trajectory dynamic pressure

C. MPCV Abort Fight control

A successful abort relies on the ability of the flight control system to maintain and control the LAV attitude at all times. This is necessary to first, ensure that the required trajectory is achieved and second, to place the crew module within the required attitude and rate envelope to ensure a successful parachute system deployment and safe landing. For LAV aborts, the flight control system's only effector is the attitude control motor. While the details of the non-linear flight control law are beyond the scope of this paper, at a very high level the vehicle pitch and yaw attitude is controlled directly by varying thrust and thrust direction of the ACM, while LAV roll is controlled indirectly by introducing a sideslip angle and utilizing the resulting aerodynamic sideforce acting in conjunction with the vertically offset center of mass providing the desired roll moment. Details of the flight control system can be found in the work by Proud et al.,,[1] and McNamara et al.[2]

The gross control torque available to the control system from the ACM is a function of the moment arm from the ACM nozzles to the current vehicle center of mass as well as the maximum directional thrust capability of the ACM. This maximum thrust is a function of the current motor operating conditions – primarily the chamber pressure, atmospheric pressure, and operation of "valves", referred to as pintles, in each of the eight ACM nozzles. All of these factors are mathematically modeled within the GN&C simulations.

The primary disturbances present during the LAV abort that the ACM must overcome to maintain controlled flight occur from two sources. First, thrust induced moments that are generated from any offset of the AM thrust vector from the center of mass. Since a large amount of propellant is consumed by the

AM and ACM during the abort, and both are located forward of the vehicle center of mass, the center of mass moves over 20 inches aft during the abort. This requires modeling of the mass properties of the LAV as a function of time for the abort simulations. The AM nozzles are not top/bottom symmetric and are designed to produce a thrust vector that when combined with the AM thrust profile, produces a time-integrated disturbance torque impulse that minimizes cases in which the ACM is unable to maintain the desired trajectory. The second primary disturbance torque is from the LAV aerodynamics, and this torque and its effect of the controllability of the LAV will be the focus of the remainder of this paper.

D. Aerodynamic Characterization of the LAV

Characterization of the LAV aerodynamics requires a highly dimensional space, including dependence on the typical aerodynamic factors of Mach number, Angle of Attack, Sideslip angle, and dynamic pressure. Since the ACM and AM plumes interact with the flowfield around the LAV, the LAV aerodynamics are also dependent on parameters relating to the operation of the motors, including gross thrust for both the AM and ACM, and both net thrust and thrust direction for the ACM. Aerodynamic forces and moments typically scale with dynamic pressure while the gross control moment produced by the ACM is independent of dynamic pressure. Due to the extremely high dynamic pressure values in some abort situations, the aerodynamic disturbance torque can be a large fraction of, or even exceed, the gross control torque produced by the ACM. These regions are obviously an area of interest and are studied, however, to allow accurate flight simulations for all conditions an aerodynamic database covering the entire flight envelope must be developed.

For the MPCV program, a mix of ground based aerodynamic testing and computational methods was used to evaluate the LAV aerodynamics. Wind tunnel testing focused on the first few seconds of the LAV flight when the AM and ACM motors were firing and the vehicle was at low angle of attack. Computational Fluid Dynamics (CFD) was used for high angles of attack during the LAV reorientation to place the CM in position for parachute deploy, and also to look at the effects of the LAV plumes at wind tunnel conditions vs. flight conditions. Modeling the LAV and plumes is a challenge for both CFD and wind tunnels - cost constraints, model size and complexity limitations, and test facility constraints limited the testing performed to warm air as the gas used to simulate the hot rocket motor exhaust of the AM and ACM plumes. These constraints also prevented testing of the LAV at flight like conditions, and as such, scaling of both inertial and plume properties had to be used resulting in a less than perfect match. CFD analysis does not have these same limitations and constraints, but limitations in turbulence modeling of both the high energy plumes and the base flow of the LAV limits the accuracy achievable for these flows. As a result, both the CFD and ground based wind tunnel testing (WTT) data were employed and combined in order to build the final aerodynamic database, with the differences between the two methods being used to partially inform the development of the uncertainty model supplied along with the database "nominal" values.

The remainder of this paper will discuss the computational simulation of the aerodynamics of the LAV during abort flight using the OVERFLOW[3,4] overset Navier-Stokes structured grid solver, discuss the physics of the interaction of the AM and ACM plumes with the flowfield around the LAV, and show the effect of this interaction on the vehicle aerodynamics and thus the control margin available to the flight control system.

II. LAV Simulations

A. Grid generation

The overset grid systems used for the analysis of the LAV are generated using an automated grid-generation process built up using the scripting system in the Chimera Grid Tools software package,[5,6] version 2.1. This script system has been coded to automatically generate the surface and volume grids, generates input files for and execute pegasus5[7] then generate the inputs files for Overflow and post-processing programs. The system has also been coded with scripts to generate the powered-face boundary-condition files needed to simulate the AM and ACM jets at various thrust conditions. The surface grids for the LAV are shown in Figures 4- 5.

The overall grid resolution was initially determined by a rigorous grid resolution study (AR ref?). Many other improvements have been made since then due to detailed analysis that showed inadequate resolution in specific areas. For example, the stream-wise resolution at the lip on the aft end of the vehicle was increased by almost a factor of ten to more accurately capture the expansion and match wind tunnel pressures in that

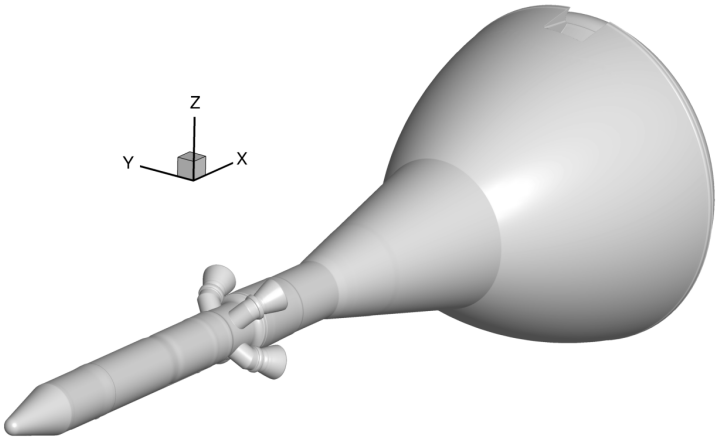

Figure 4. LAV surface

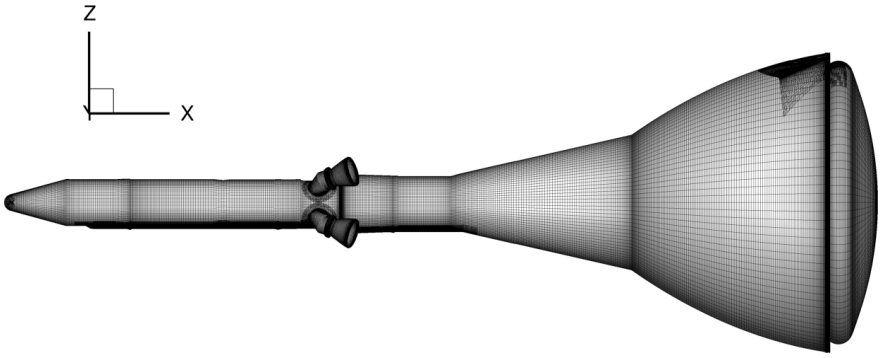

Figure 5. LAV surface grids

region. See Figure 6 for a closeup of the grid on the aft lip. Another area in which the grid resolution was increased is the AM lip and plume refinement grids. Detailed comparisons to the AM power on wind tunnel tests showed that the CFD wasn't capturing the correct physics due to, among other things, a lack of grid resolution (AR refs?). Figure 7 shows the AM nozzle and raceway details. Note the very high stream-wise resolution at the nozzle lip.

There are a number of different ACM jet configurations simulated using the Overflow code. One example is a max-thrust ACM during the AM burn. In this case, two adjacent ACM nozzles are at full thrust with the remaining 6 ACM nozzles closed and the AM fires at full power through all four AM nozzles. The grid system for this configuration includes only the two power-on ACM nozzles, with the other ACM nozzles faired over to reduce the number of grid points required. In order to accurately model the ACM, two grid zones were generated for each ACM nozzle: a cylindrical nozzle-fitted grid which wraps from the inside of the nozzle and up onto the outer surface of the LAV, and an overlapping grid inside the core of the nozzle. A close-up of the surface grids in the vicinity of the ACMs and a cross-section of one of the ACM nozzles is shown in Figure 8.

The modeling requirements of the AM nozzles are similar to the ACM, and the same body-fitted grid and overlapping core grid are used. In addition to these grids there several plume refinement grids. For each AM nozzle, there is a near-nozzle plume refinement grid that extends 4 nozzle diameters in the axial direction. The radial spacing near the AM lip is very fine and is intended to capture the AM plume shear layer. The spacing in the radial direction becomes uniform at the downstream end of the near-nozzle plume refinement grid. The axial spacing near the AM lip is the same as the radial spacing, resulting in roughly square cells at the nozzle lip, and increases to a larger value at the downstream boundary. A two-dimensional version of this grid is built and revolved about the nozzle symmetry axis with uniform spacing in the circumferential

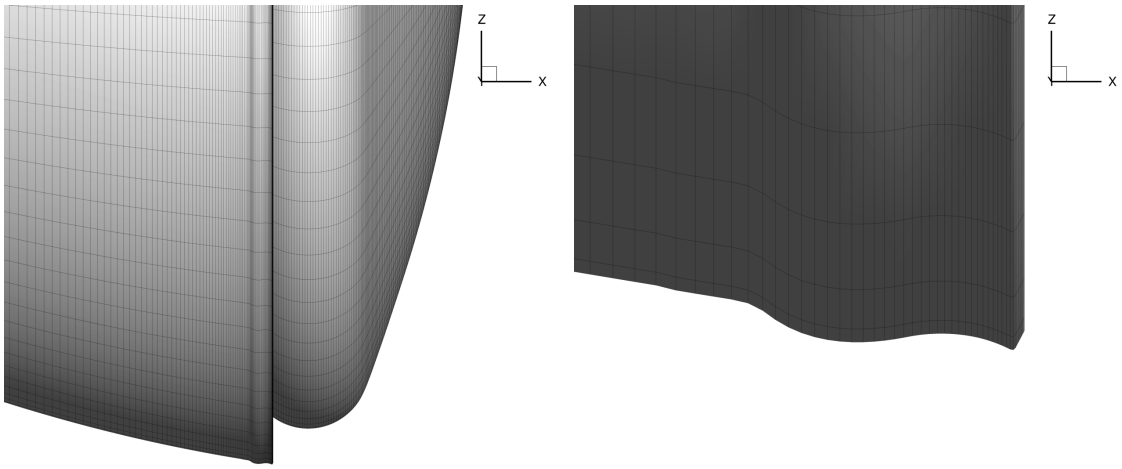

Figure 6. LAV aft lip

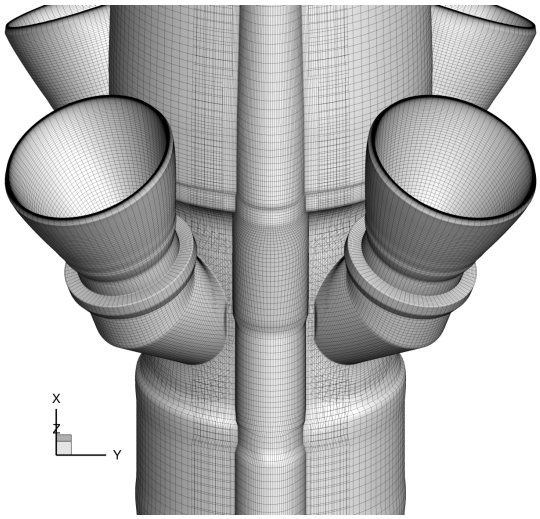

Figure 7. LAV AM and raceway

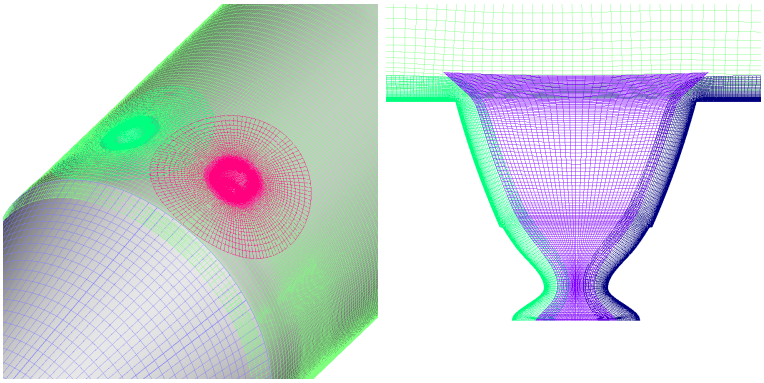

Figure 8. Attitude control motor nozzle geometry and plume refinement grids

direction. The axis is removed and replaced with an overlapping core grid, similar to what is done with the nozzle-fitted grid. The flow gradients from the four near-nozzle plume refinement grids are carried downstream by a single far-nozzle plume refinement grid. This grid is very similar in topology to the near-nozzle grids but instead is revolved about the vehicle's X-axis. See Figure 9 for an illustration of the nozzle geometry and the plume refinement grids.

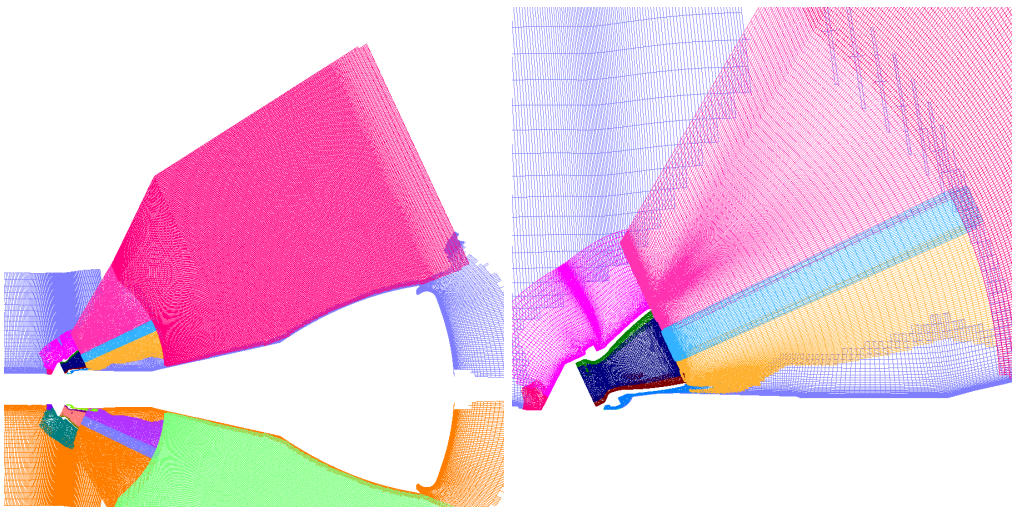

Figure 9. Abort motor nozzle geometry and plume refinement grids

The grid systems typically contain on the order of 60 zones and approximately 90 million grid points. There are approximately 33 million grid points in the abort motor plume refinement grids alone.

B. Computed results

The modeling discussed in this paper is performed using the Overflow code, which uses a structured overset-grid approach and solves the Reynolds-averaged Navier-Stokes equations. An extensive amount of work has been performed to develop guidelines on the best methods to model the LAV. These, as well as some of the computational results for this vehicle are documented by in previous works by the current authors.[8–11]

Computing the aerodynamics of the LAV, and in particular the jet-interactions due to the AM and ACM plumes over the entire parametric space required by the aerodynamic database proved to be very challenging. In covering this envelope with test and analysis, a number of non-linear behaviors have been uncovered. This section will briefly discuss the effects of the AM and ACM with a particular emphasis placed on how the jet-interaction affects the control of the LAV.

The AM effects on pitching moment is a strong function of the vehicle Mach number, as well as the AM thrust coefficient (C_T), which is defined as the AM thrust normalized by the freestream dynamic pressure and vehicle reference area resulting in a non-dimensional thrust coefficient similar to that of Drag Coefficient (C_D). To illustrate this non linear behavior, Figure **??** shows the variation of the LAV pitching moment derivative with respect to Alpha (C_m-alpha) vs Mach number at constant thrust coefficient of 2, 3, and 4.

Typically a negative value of C_m-alpha is desired as this will result in increasing restoring moment as the vehicle attitude moves farther from the trim condition and thus result in static stability. It should be noted, however, that this correlation of C_m-alpha and stability will only hold if the vehicle has locally linear aerodynamics and only for C_m-alpha computed around the trim point. It it is common for vehicles to have areas of positive C_m-alpha away from a trim condition but remain stable due to the overall magnitude of restoring torque being stabilizing even though the slope is not negative. Without any AM or ACM plumes, shown as "power off" (black line) in Figure **??**, the LAV does have a desirable negative C_m-alpha for all Mach numbers. With the AM active, however, the plumes from the 4 aft facing nozzles at the midpoint of the LAV tower interact with the freestream flow and change the aerodynamics of the vehicle and produce an unstable pitch slope. The region in Mach number at which this instability occurs, and the magnitude is a function of the AMCT. At a CT ration of 2, the pitch moment slope is unstable from Mach 1.05 to 2 and at again at Mach 6, and at all Mach numbers the AM jet-interaction is either almost zero effect, or is detrimental to overall vehicle stability, with the stability being most affected in the high transonic range where dynamic pressures tend to also be largest.

Moving up in thrust to a CT ratio of 3.0, the instability produced by the AM jet-interaction is larger in magnitude, but occurs in a narrower range of Mach number – from 1.1 to 1.8 – as shown in Figure **??** by the . At this power condition, the AM effect is destabilizing at all Mach numbers with the exception of 2.0 where there is almost no effect relative to the power off value.

At a thrust coefficient of 4.0 the level of instability again grows larger, but is further compressed in Mach number to below 1.4 as shown in Figure **??**. Looking at all three CT value plots - one can see that the pitch slope increases before reaching a minimum, then increasing again as the vehicle accelerates toward Mach 6 but the location of these increases and minimums are compressed toward the low Mach range with increasing CT. As a result, the higher CT conditions exhibit a much more non-linear aerodynamic response to Mach number.

In addition to this nonlinearity with Mach number, in characterizing of the plume effects of the LAV, a strong dependence of the aerodynamics to the plume thrust coefficient at a fixed Mach number was also discovered. This behavior is in large part driven by the shape of the AM plumes changing as a function of CT. The AM plumes are, at most flight conditions, comprised of several shock cells that are formed as the plume initially expands out of the nozzle toward the lower ambient conditions and then turns back inward necessitating a strong shock. This defines the first shock cell, and following this strong shock the central pressure in the plume core is again higher than ambient conditions and the plume again expands and starts the cycle again. The length and size of these shock cells is dependent on the AM chamber pressure and the freestream conditions into which the plume is flowing. As the AM plumes are largest in diameter at a point approximately halfway between the strong shocks, and narrowest at these shocks, movement of these features changes the distance between the LAV surface and the very high velocity/ high energy shear layer of the plume. Interaction between these plumes and the surface results in drastic changes in surface pressure on the ogive and thus drives large variations in the vehicle stability. Figure 13 shows the plume shape as CT is increased from 2.0 to 6.0 at a flight condition of Mach 0.7 and 10 degrees angle of attack. The effect of the plume as it passes near the ogive is to create a region of low pressure since the much higher velocity of the plume core entrains flow between it and the ogive, acting as ejector and resulting in a localized

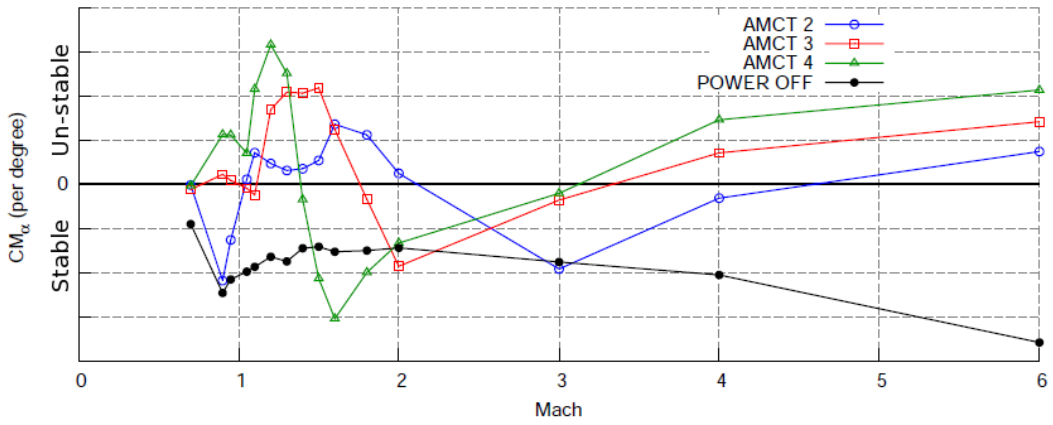

Figure 10. LAV Pitch Stability with and without AM firing

low pressure area. In conditions where the plume core impinges directly on the the LAV surface, the high energy in the plume creates a region of high pressure. For the conditions shown in Figure 13 the plume core passes sufficiently close to the ogive to create a large region of low pressure on the ogive. For the freestream condition pictured, this low pressure region closely tracks the maximum diameter of the 3rd shock cell as CT is increased. The 3rd shock cell moves aft of the vehicle between CT=5 and CT=6, with a new low pressure area forming at CT=6 near the 2nd shock cell maximum diameter which is now in proximity to the LAV ogive due to the increasing pressure ratio between the nozzle and the freestream pressure.

As these changes in surface pressure can be, and often are, very large in magnitude and affected area, small asymmetries between pairs of plumes can have large impacts on the vehicle stability. The integrated effect of these large pressure changes for the most part cancel each other out as the opposing plumes behave grossly similar, but small asymmetries between pairs of plumes can have large impacts on the vehicle stability due to the large magnitude of pressure change and the large area affected. Figure 14 shows the integrated effect of the surface pressure changes due to the AM plumes interacting with the LAV similar to that shown above in Figure 13. Note that for all thrust coefficient values the jet-interaction increment is positive, and thus destabilizing. In addition, the behavior is very nonlinear - the selected points for analysis being separated by at most 0.25 CT are not fully sufficient to define the shape of the curve. This is especially true for the Mach 1.1 condition from CT=0.75 to 2.5 where the pitching moment increment goes through 5 reversals of slope.

Unfortunately, asymmetry between the pairs of plumes are in effect built into the LAV, as the Crew module center of mass is offset in order to produce a trim angle of attack to give a lift to drag ratio of approximately 0.25. This allows the CM to lower entry loads placed on the crew relative to a pure ballistic entry, and also allows downrange targeting so that the recovery area is a small fixed region instead of having to cover large areas of ocean with many costly recovery vessels and crews. This offset center of mass moves the LAV center of mass off of the centerline and requires that the AM thrust vector be canted slightly to reduce the torque produced during the AM burn. This is done by placing slightly smaller nozzles throats on the nozzles opposite of the offset mass center. This slightly reduces their thrust relative to the other 2 nozzles and cants the resultant thrust vector of all 4 nozzles so that its line of action passes closer to the center of mass and reduces the disturbance torque. As a result however, the plumes opposing each other have slightly different pressure ratios, and the shock cell structure and plume diameter, etc. are not symmetric.

Other factors also influence the jet-interaction. At angle of attack, the AM plumes on the windward side will be more directly exposed to the freestream flow and will be pressed toward the center of the vehicle more than their counterparts on the leeward side. In addition, for supersonic flows, the shockwave that forms in front of the AM plumes will be stronger on the windward side of the vehicle, creating a higher pressure into which the AM plumes expand. This will change the pressure ratio and thus the shock cell formation of the AM plumes.

The maximum pitch up moments (unstable) are created at CT=1.5 and 2.5 with the AM induced pitching moment increment swinging from near zero at CT=2, to approximately 0.036 at CT=2.5. At a CT=2.5

Figure 11. AM Plume Flow Visualization for Mach = 0.70, $\alpha = 10^{\circ}$

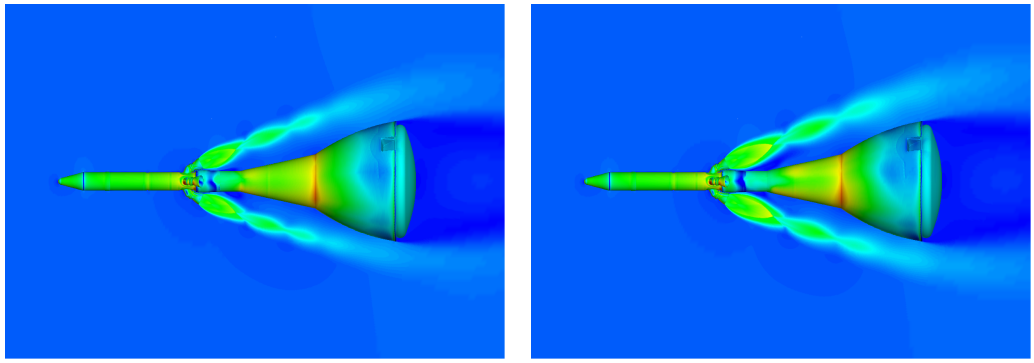

(a) AMCT=2

(b) AMCT=3

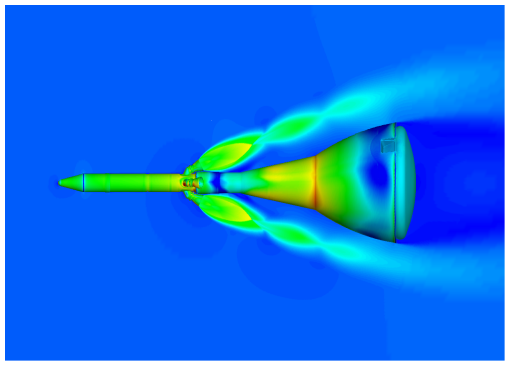

(c) AMCT=3.5

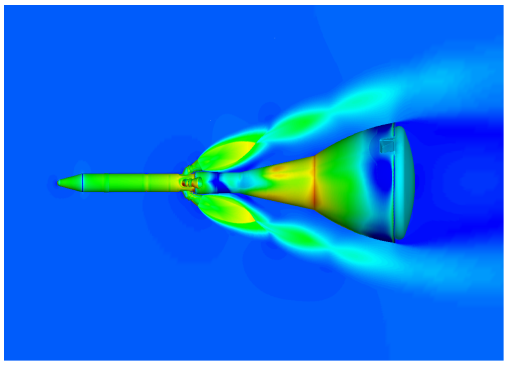

(d) AMCT=4

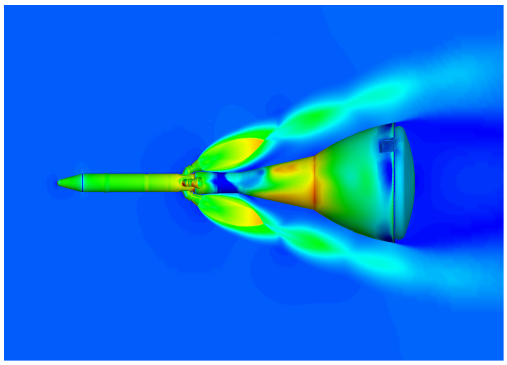

(e) AMCT=5

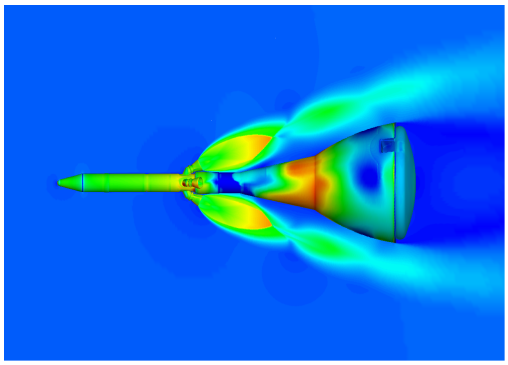

(f) AMCT=6

assuming full AM thrust, the dynamic pressure is only in the neighborhood of 740, so the ACM has a C_m authority of approximately 0.09. This means that negating the AM interaction requires 40 percent of the theoretical thrust capability of the ACM.

Additionally, the firing of the ACM creates changes to the pressure field downstream of them, affecting the AM plumes. These changes are functions of thrust magnitude as well as direction and have proven hard to fully characterize.

C. ACM and AM Interactions

This section highlights some of the computed results in which both the ACM and AM jets are firing. The goal of these simulations is to provide ACM jet-interaction increments in the forces and moments. These increments are measured as the difference between firing both the ACM and AM jets versus firing just the AM jets. The eight ACM nozzles are arranged 45 degrees apart circumferentially in an axial location just

Figure 12. AM Plume interaction vs. CT at $\alpha = 10°$

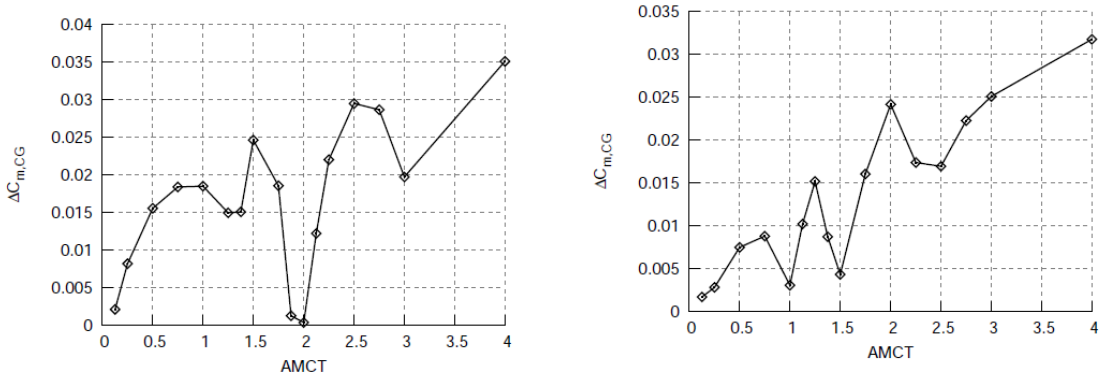

(a) Mach 0.9

(b) Mach 1.1

aft of the LAT nose. The nozzles are equally spaced 22.5 degrees on either side of the pitch and yaw planes of the vehicle. The ACM system parameters include the resultant-thrust direction, the thrust balance, and the ACM thrust ratio. The thrust direction describes the circumferential angle of the resultant thrust vector relative to the +Z pitch plane. The thrust balance is the ratio of the resultant-thrust magnitude to the total system thrust, and the thrust ratio is the total system thrust divided by the product of the freestream dynamic pressure and the vehicle's reference area. The thrust from each of the eight ACM nozzles can be controlled independently using pintle valves, under the constraint that the ACM solid-motor exhaust must be vented through at least two or more of the nozzles. The three ACM parameters can be commanded to many thousands of configurations. Only a small fraction of the configuration space was studied using CFD simulations. Only one combination of these parameters is presented here: the ACM thrust-direction is along the +Z body axis, the thrust balance is set to 1.0, and the thrust ratio is 0.04. This configuration uses equal thrust through the two nozzles on either size of the pitch plane on the -Z side of the LAT.

Figures 15 and 16 show the computed ACM pitching-moment effectiveness plots versus angle of attack for the different freestream Mach conditions. Each plot has different curves for the different values of AM thrust coefficient. The ACM pitching-moment effectiveness Eff_{Cm} is defined as:

$$Eff_{Cm} = 1 - \frac{CMJI}{CMJT}$$

$$CMJT = Cm_{total\_no\_thrust} - Cm_{total}$$

$$CMJI = Cm_{total\_no\_thrust} - Cm_{ACMoff}$$

where $Cm_{total\_no\_thrust}$ is the pitching moment without including the ACM thrust components, Cm_{total} is the pitching moment with the ACM thrust component included, and Cm_{ACMoff} is the pitching moment for the corresponding ACM power-off case. Values of Eff_{Cm} near 1.0 indicate that the jet interference is small relative to the moment provided by the ACM jets. Values well below 1.0 indicate a significant jet interference, and if the effectiveness goes to zero, then the ACM-jet interference exactly offsets the moment produced by the jets at the given conditions. Negative effectiveness indicate a control reversal. These figures show that the lowest effectiveness tend to occur at Mach=0.90, AMCT=4, and at Mach=1.1, AMCT=3, and at Mach=1.6, AMCT=4.

The following figures illustrate the flow-field around the vehicle with the AM firing, both with and without the ACM jets firing in the pitch-up maneuver. These figures color the surface of the vehicle with pressure coefficient contours, and include contours of local Mach number in a cutting plane immediately aft of the vehicle. They also show a Y-cutting plane through the center of the starboard-side AM nozzles in which are drawn gray-scaled contours of the log of density-gradient magnitude. Also included are semi-transparent iso-surfaces of Mach number used to illustrate the plumes from the AM and ACM nozzles.

At Mach=0.9 and α=5, the ACM effectiveness is very low. The flow-field plots in Figure 17 illustrate both the ACM-on and ACM-off solutions for CT=2, Mach=0.9, α=5. These show that the ACM plumes

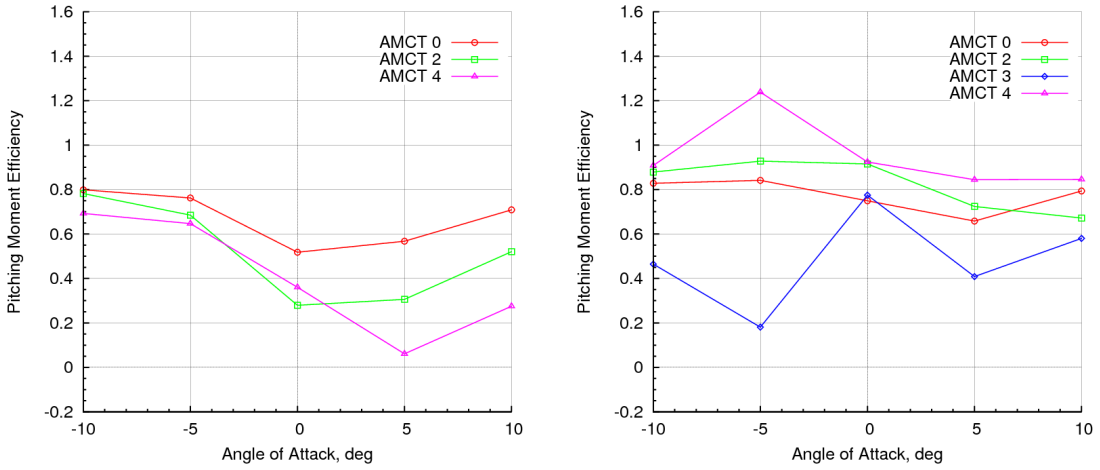

Figure 13. ACM effectiveness versus angle of attack for freestream Mach numbers of 0.9 and 1.1

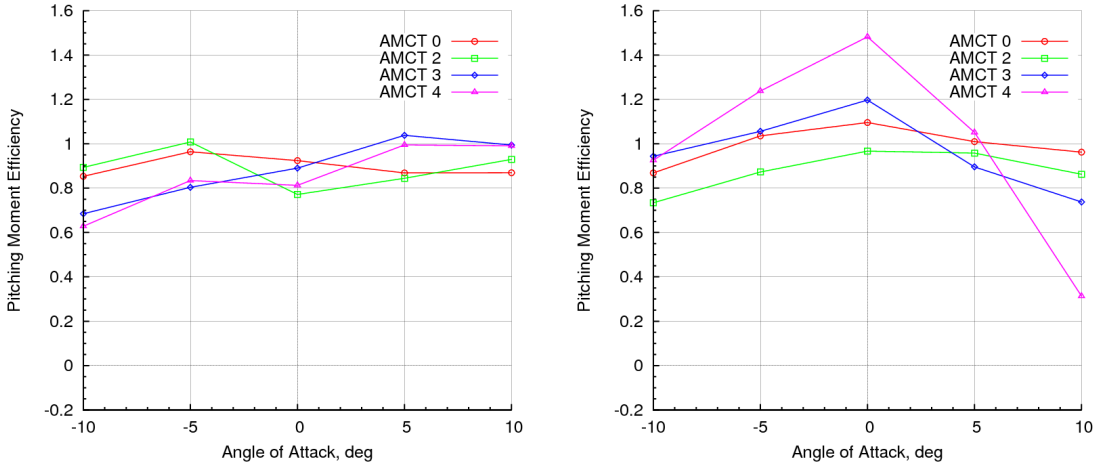

Figure 14. ACM effectiveness versus angle of attack for freestream Mach numbers of 1.3 and 1.6

change the interaction of the bottom two AM plumes with the LAV ogive, referred to as the boost protective cover or BPC. It appears that the ACM plumes block the on-coming freestream flow such that the AM plumes remain further away from the LAV ogive than in the ACM-off solution. The slight difference in the location of the AM plumes is evident in the Mach contours directly aft of the heatshield, and in the plume iso-surfaces. When the AM plumes brush closer to the BPC lower surface, the pressure contours show lower pressure on the bottom of the BPC, and higher pressure when the AM plumes are further from the BPC. This higher pressure on this region of the BPC in the ACM-on solution causes more of a nose-down, or lower, pitching moment compared to the ACM-off solution. This nose-down pitching moment acts counter to the nose-up pitching moment imparted by the force of the ACM jets. Thus the pitching-moment effectiveness is low in this case. Figure 18 shows solution plots at the same conditions except with CT=4. This higher AM thrust is evident in the larger AM plumes. These two images show a similar ACM jet interaction occurring, and because of the larger AM plumes, it appears to affect a larger area on the BPC. As a result, the ACM effectiveness is even lower in this case.

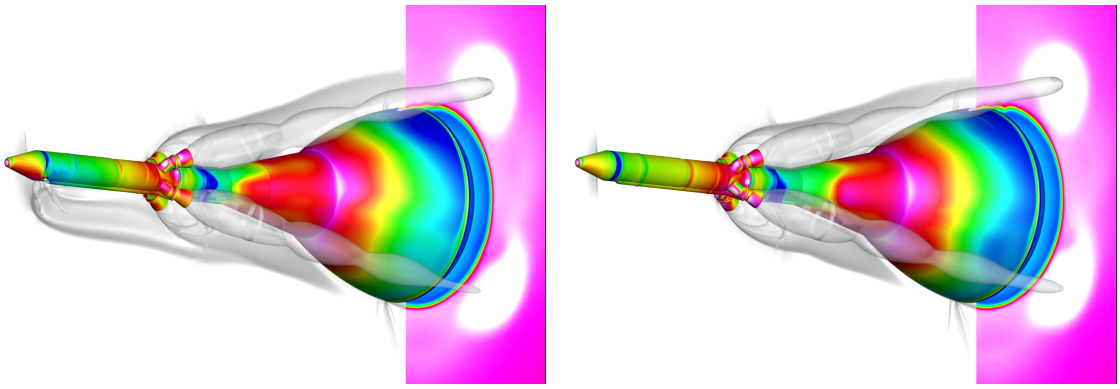

Figure 15. Flow-field plots of ACM-on and ACM-off solutions for CT=2, Mach=0.9, and α=5

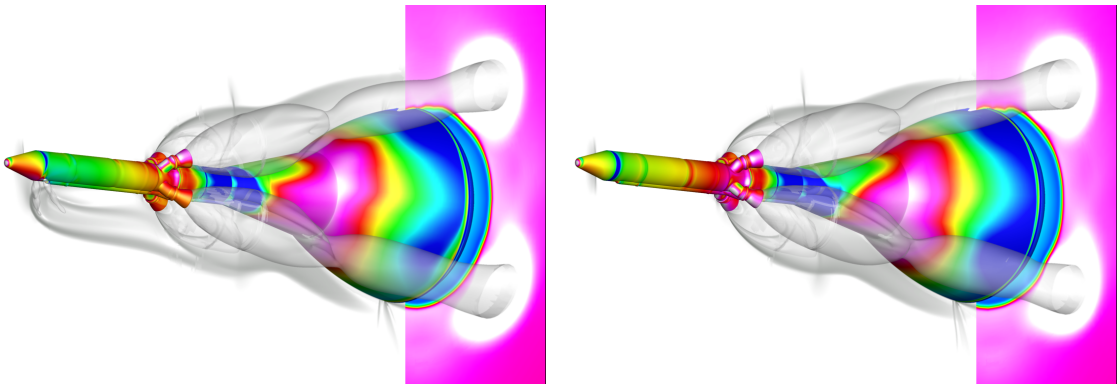

Figure 16. Flow-field plots of ACM-on and ACM-off solutions for CT=4, Mach=0.9, and α=5

In figures 20 through 24 several solutions at Mach=1.1 are shown. These transonic cases all show a normal shock near the nose of the vehicle, and a normal shock at the front end of the BPC where the cross-sectional area of the vehicle is rapidly increasing. The BPC shock causes the AM plume to undergo a sharp reduction in size. Figure 19 is a plot with Mach contours in a 45-degree cutting plane through the center of the AM nozzles and a stream-wise constant plane just aft of the heat-shield. Also shown are gray-scaled surface pressure-coefficient contours where the lowest surface pressure is colored with dark blue. This is from the Mach=1.1, α=5, CT=4 solution. This figure illustrates the effect of the BPC shock on the AM plumes. Aft of this the AM plumes expand again causing them to contact the aft portion of the BPC, resulting in regions of low surface pressure. Small changes in angle of attack, AM thrust, and ACM interactions can result in big changes in the vehicle forces and moments depending on the AM plume interaction with the BPC.

In figures 20 and 21 the solutions for Mach=1.1 and α=-5 are plotted for AM thrust values of CT=3 and CT=4, respectively. The CT=3 case has very low pitching-moment effectiveness, while the CT=4 case has a value greater than 1.0. The figures show that the CT=3 ACM-off case has low pressures on the bottom-aft end of the BPC caused by the AM plumes, but turning on the ACMs eliminate this low pressure, resulting in a strong nose-down pitching moment and low ACM effectiveness. However with the larger AM plumes in the CT=4 solution, this effect is reversed, and the ACM effectiveness is greater than 1.0. In figures 22, 23, and 24 the solutions for Mach=1.1 and α=5 are shown for values of CT=2, CT=3, and CT=4, respectively. Similar effects are seen in the ACM interactions, where the increasing AM thrust levels reverse the effect of the ACM interactions.

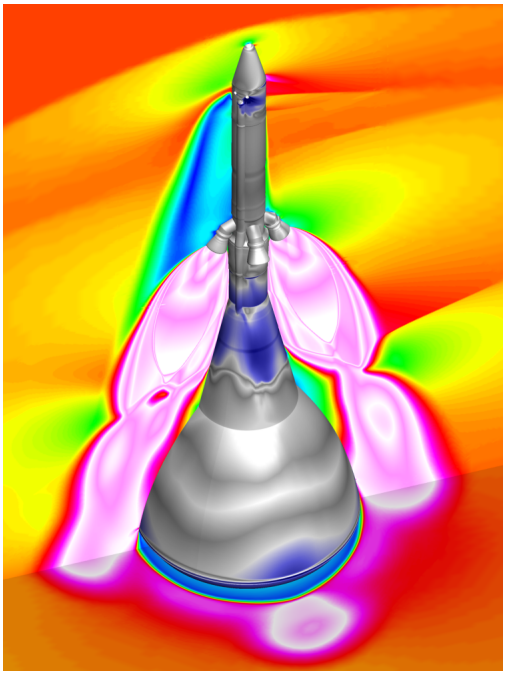

Figure 17. Off-body Mach contours and surface pressure-coefficient contours for ACM-on solution at CT=4, Mach=1.1, and α=5

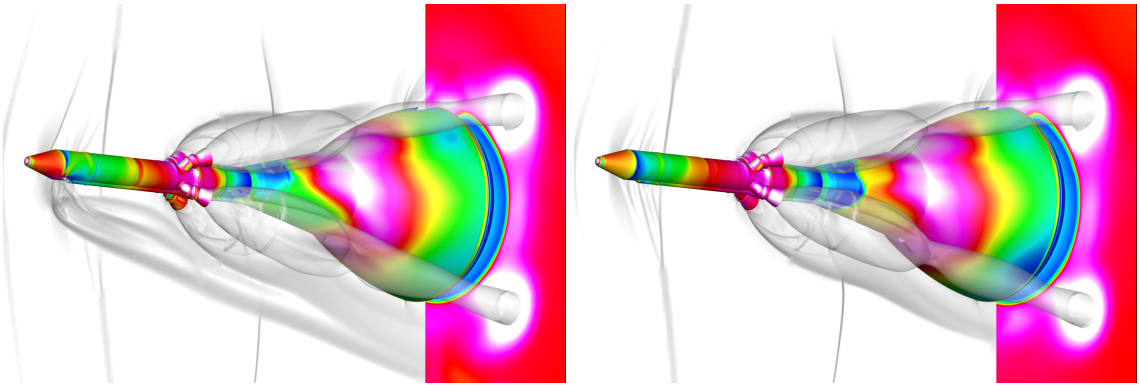

Figure 18. Flow-field plots of ACM-on and ACM-off solutions for CT=3, Mach=1.1, and α=-5

The solutions at Mach=1.6 and CT=4 are shown in figures 25 and 26, for α=0 and α=10, respectively. Recall that figure 16 showed that the α=0 case has an effectiveness greater than 1.0, while the α=10 case is significantly less than 1.0. At α=0 several effects of the ACM plumes are evident at this supersonic speed. The ACM plumes changes the location of the shock caused by the AM nozzles and plumes, and this causes higher pressure on the lower AM nozzles and lower pressure on the upper AM nozzles. This increases the nose-up pitching moment. The interaction of the AM plumes with the BPC is also altered, such that the

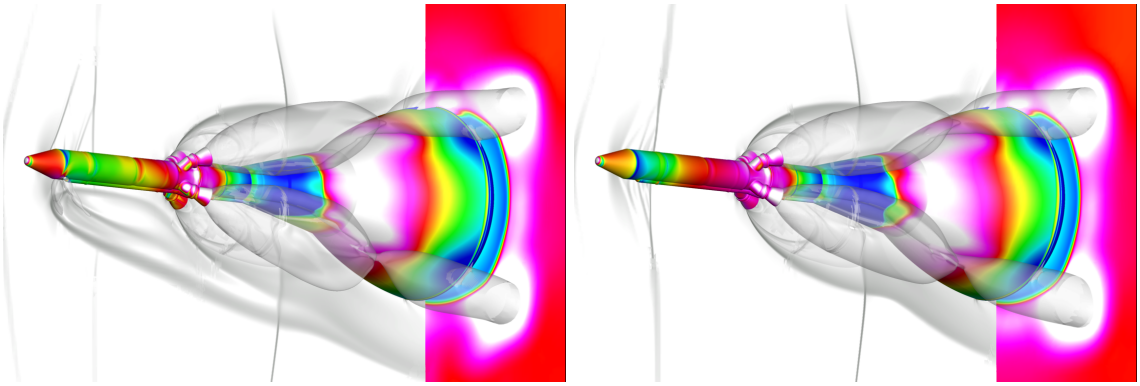

Figure 19. Flow-field plots of ACM-on and ACM-off solutions for CT=4, Mach=1.1, and α=-5

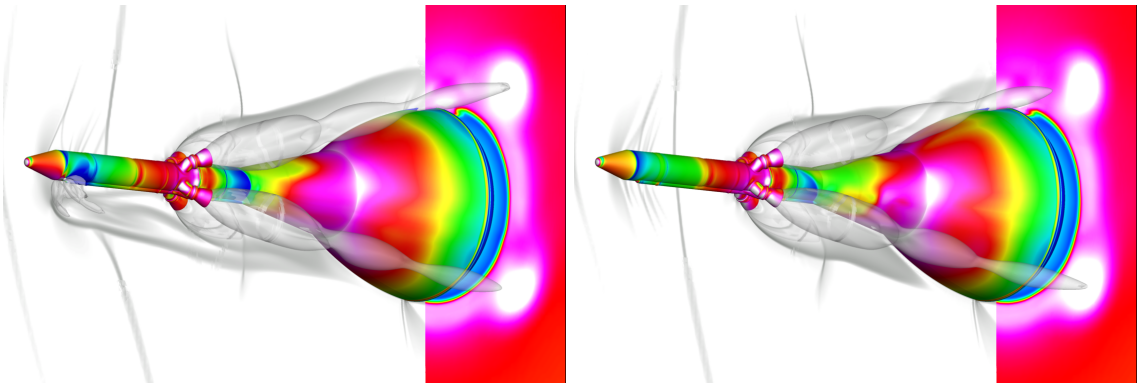

Figure 20. Flow-field plots of ACM-on and ACM-off solutions for CT=2, Mach=1.1, and α=5

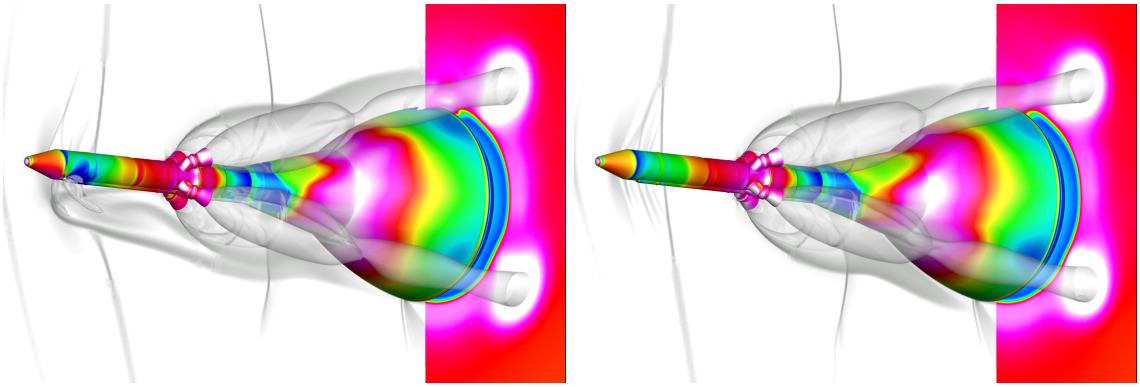

Figure 21. Flow-field plots of ACM-on and ACM-off solutions for CT=3, Mach=1.1, and α=5

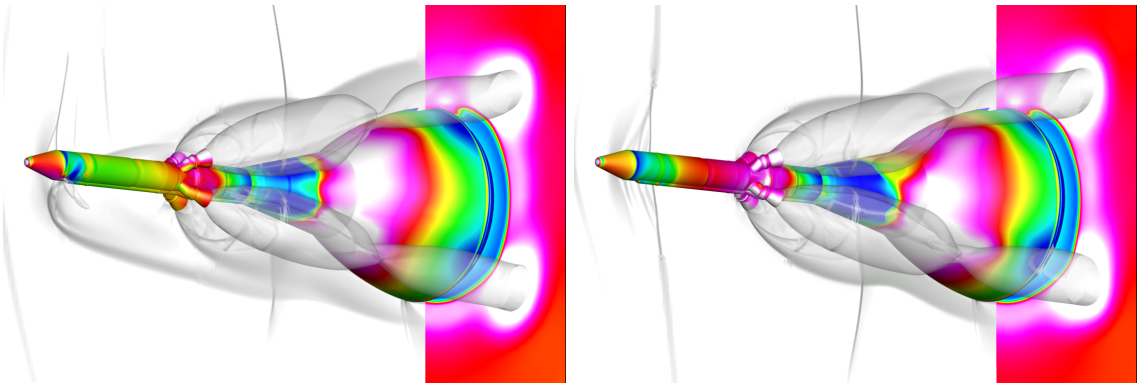

Figure 22. Flow-field plots of ACM-on and ACM-off solutions for CT=4, Mach=1.1, and α=5

lower AM plumes generate lower pressure on the BPC, also increasing the pitching moment. Thus at these conditions, the ACM jet interaction enhances the pitching moment. The α=10 solutions also show a change in the shock locations when the ACMs are firing. At this angle of attack, however, the opposite effect is seen on the pressure on the AM nozzles. There is also a larger area of low pressure on the tower just aft of the ACM nozzles, causing a nose-down pitching moment. Finally, the impingement of the AM plumes on the BPC causes higher pressures when the ACMs are firing, which also creates a nose-down pitching moment. These all contribute to the low ACM effectiveness at this condition.

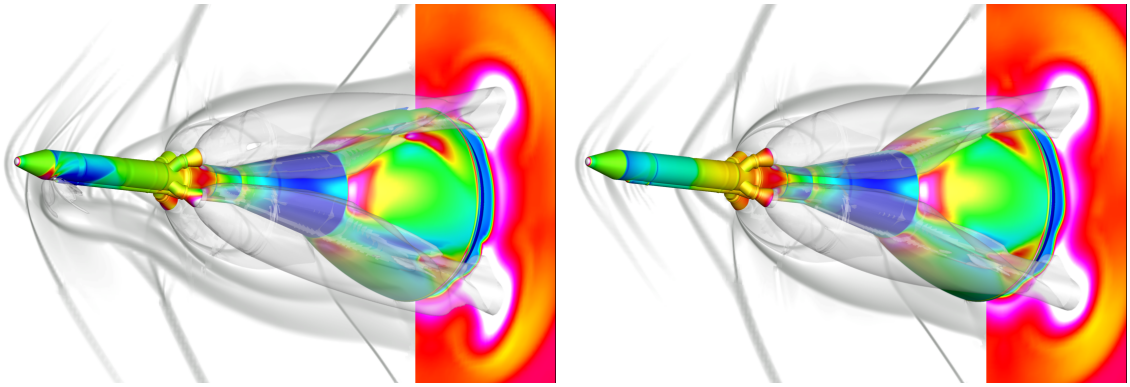

Figure 23. Flow-field plots of ACM-on and ACM-off solutions for CT=4, Mach=1.6, and α=0

III. Conclusion

References

[1]R. W. Proud, J. R. Bendle, M. B. Tedesco, and J. J. Hart, "Orion Guidance and Control Ascent Abort Algorithm Design and Performance Results", Document Number AAS09_092, Proceedings of the 32nd Annual AAS Guidance and Control Conference, February 2009

[2]S. J. McNamara, C. I. Restrepo, E. A. Medina, R. J. Whitley, J. M. Madsen, and R. W. Proud, "Gain Scheduling for the Orion Launch Abort Vehicle Controller", AIAA Paper 2011-6259, Aug 2011.

[3]P.G. Buning, R.J. Gomez, and W.I. Scallion, "CFD Approaches for Simulation of Wing-Body Stage Separation," AIAA Paper 2004-4838, AIAA 22nd Applied Aerodynamics Conference, Providence, RI, Aug. 2004.

[4]Jespersen, D. C., Pulliam, T. H., and Buning, P. G., "Recent enhancemnts to OVERFLOW," AIAA Paper 97-0644, Jan. 1997.

[5]Rogers, S. E., Roth, K., Nash, S. M., Baker, M. D., Slotnick, J. P., Whitlock, M., and Cao, H. V., "Advances in Overset CFD Processes Applied to Subsonic High-Lift Aircraft," AIAA Paper 2000-4216, Aug. 2000.

[6]Chan, W. M., "The Overgrid Interface for Computational Simulations on Overset Grids," AIAA Paper 2002-3188, June 2002.

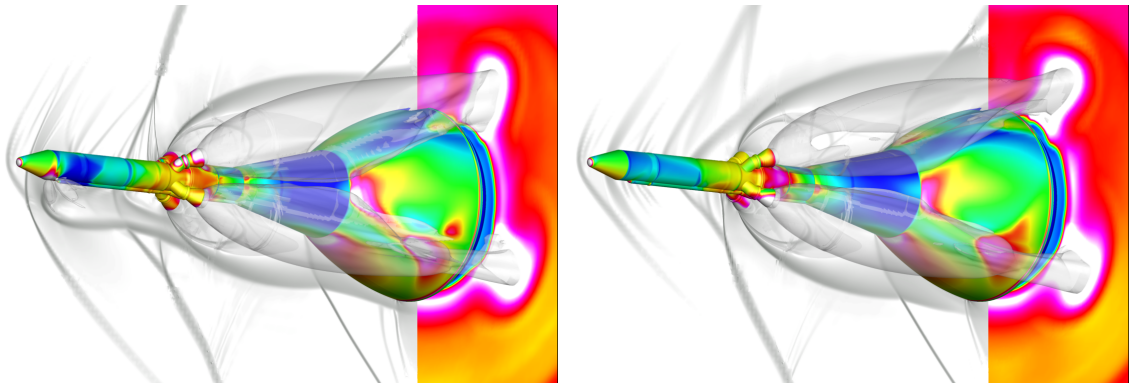

Figure 24. Flow-field plots of ACM-on and ACM-off solutions for CT=4, Mach=1.6, and α=10

[7]Rogers, S. E., Suhs, N. E., and Dietz, W. E. "PEGASUS 5: An Automated Pre-processor for Overset-Grid CFD," *AIAA Journal*, Vol. 41, No. 6, June 2003, pp. 1037–1045.

[8]Aftosmis, M. J. and Rogers, S. E., "Effects of Jet-Interaction on Pitch Control of a Launch Abort Vehicle", AIAA Paper 2008-1281, Jan. 2008.

[9]Rogers, S. E. and Pulliam T. H., "Computational Challenges in Simulating Powered Flight of the Orion Launch Abort Vehicle," AIAA Paper 2011-3339, June 2011.

[10]Childs, R., Garcia, J., Melton, J., Rogers, S. E., Shestopolov, A., and Vicker, D., "Overflow Simulation Guidelines for Orion Launch Abort Vehicle Aerodynamic Analysis," AIAA Paper 2011-3163, June 2011.

[11]Childs, R., Rogers S., "Overflow Aerodynamic Simulation of the Orion Launch Abort Vehicle", JANNAF Paper xxxx-xxxx, Dec 2012.